

Enhancing Image Restoration Transformer via Adaptive Translation Equivariance

JiaKui Hu^{1,2,3}, Zhengjian Yao^{1,2,3}, Lujia Jin⁴, Hangzhou He^{1,2,3}, Yanye Lu^{1,2,3*}

¹Institute of Medical Technology, Peking University Health Science Center, Peking University

²Biomedical Engineering Department, College of Future Technology, Peking University

³National Biomedical Imaging Center, Peking University

⁴China Mobile Research Institute

jkhu29@stu.pku.edu.cn, yanye.lu@pku.edu.cn

Abstract

Translation equivariance is a fundamental inductive bias in image restoration, ensuring that translated inputs produce translated outputs. Attention mechanisms in modern restoration transformers undermine this property, adversely impacting both training convergence and generalization. To alleviate this issue, we propose two key strategies for incorporating translation equivariance: slide indexing and component stacking. Slide indexing maintains operator responses at fixed positions, with sliding window attention being a notable example, while component stacking enables the arrangement of translation-equivariant operators in parallel or sequentially, thereby building complex architectures while preserving translation equivariance. However, these strategies still create a dilemma in model design between the high computational cost of self-attention and the fixed receptive field associated with sliding window attention. To address this, we develop an adaptive sliding indexing mechanism to efficiently select key-value pairs for each query, which are then concatenated in parallel with globally aggregated key-value pairs. The designed network, called the Translation Equivariance Adaptive Transformer (TEAFormer), is assessed across a variety of image restoration tasks. The results highlight its superiority in terms of effectiveness, training convergence, and generalization.

1. Introduction

Image restoration aims to reconstruct high-quality (HQ) images from their low-quality (LQ) counterparts, which are often affected by degradations resulting from the imaging system or environment. As a constituent of the imaging system, image restoration methods should satisfy the following fidelity property: the restoration results for the target region should remain equivariant under geometric transfor-

mations of the input. This fidelity property is termed translation equivariance, which is one of the inherent inductive biases in image restoration.

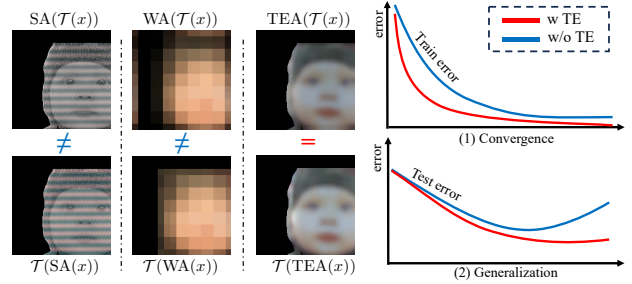


Figure 1. $\mathcal{T}(\cdot)$ means the translation function. "SA" and "WA" are commonly used for self-attention and window attention, respectively, but disrupt translation equivariance (TE) due to position encoding and feature shifting. "TEA" is our proposed translation equivariance adaptive attention, which satisfies TE. TE promotes faster convergence and better generalization.

Attentions	TE	Performance		NTK [25]	SRGA [33]	Complexity
		PSNR \uparrow / SSIM \uparrow	Condition \downarrow	Value \downarrow	Value \downarrow	
SA	✗	28.21 / 0.8435	11140.44	4.075	$\mathcal{O}(N^2)$	
WA	✗	27.45 / 0.8254	1746.49	3.655	$\mathcal{O}(N)$	
TEA (Ours)	✓	28.67 / 0.8489	236.78	3.275	$\mathcal{O}(N)$	

Table 1. In $4\times$ image super-resolution, we study performance, NTK [8] convergence speed, SRGA [33] generalization, and computation complexities. We replace WA in SwinIR with SA and TEA for testing. TEA shows fast convergence, better generalization, and linear complexity. The results are tested on Urban100.

In restoration networks [32, 62, 68, 71] based on convolution neural networks (CNNs), the paradigm of sliding information extraction inherent to convolutions [18] imparted a natural translation equivariance (TE)¹ property in restoration networks. However, as shown in Figure 1 and Table 1,

¹Translation equivariance and translation invariance are concepts that are frequently misconstrued. Our paper is dedicated to the analysis of equivariance. We have provided a clear delimitation and discussion concerning these concepts in the supplementary material.

*Corresponding author.

the advent of Self Attention (SA) [51] and Window Attention (WA) [34] within Transformers has broken this fidelity property, leading to slow convergence and poor generalization in restoration transformers.

In this paper, we propose two fundamental strategies to bring TE back into the restoration transformers: (1) *slide indexing* and (2) *component stacking*. The slide indexing strategy employs a fixed container, *e.g.*, a fixed rectangular window, to globally extract the input in a sliding fashion. This method requires the operators to calculate instantaneously, thereby maintaining the consistency of positional coordinates between the input and output of the model, which facilitates the integration of TE. The component stacking strategy involves stacking modules that satisfy the TE property in parallel or in series, thus enhancing architectures while ensuring TE in complex networks.

However, these foundational strategies present a persistent challenge in the design of restoration transformers. Selecting SA to achieve superior performance involves accepting its substantial computational complexity [63]; alternatively, opting for sliding window attention provides linear complexity but results in a fixed receptive field [48] and reduced performance. To break this dilemma, we replace the global key-value pair indexing mechanism in vanilla SA with an adaptive slide indexing mechanism to design the Translation Equivariance Adaptive (TEA) attention. To retain the extraction of global information, TEA incorporates a downsampling self-attention branch without position encoding, which reduces the key-value pair’s resolution by aggregating them, thereby providing TEA with coarse, yet effective global information.

In summary, our contributions are threefold. **First**, we investigate TE in image restoration, analyzing its impact on convergence and generalization. The results indicate that the integration of TE is essential in the design of restoration networks. **Second**, we propose TEA, which uses adaptive slide indexing methods to incorporate the TE property while preserving linear complexity and ensuring a global receptive field, thereby enhancing restoration transformers. **Third**, we introduce TEA to the vanilla Vision Transformer to design TEAFormer. Experiments show that TEA achieves State-of-The-Art (SoTA) performance in various image restoration tasks, while having faster convergence and more robust generalization.

2. Related Work

Vision Transformers with inductive bias. Following the pioneering introduction of the Transformer [51] into vision tasks by ViT [16], SA has emerged as a key component in vision networks. However, ViT is challenging to train, exhibits slow convergence, and requires substantial data support [49]. Previous works, such as ViTAE [59, 70], attributed this to a lack of inductive bias and advocated in-

tegrating inductive bias with ViT to develop more efficient ones. AACNet [4] emphasized the importance of translation equivariance for visual tasks. The Swin [34] and CSwin [15] Transformers incorporated local processing into the vision Transformer, thus proposing window attention. CVT [56] and FasterViT [21] sequentially stack convolutions and attention layers, resulting in a hybrid architecture. PVT [52, 53] used average pooling for downsampling to achieve weak translation equivariance. Both DAT [57] and BiFormer [74] dynamically determined the windows accessible to each token. Recently, some studies have introduced translation equivariance into ViT by modifying position encoding [4, 58] and attention calculation logic [44, 46].

Recent image restoration Transformers. Similar to the development of vision transformers, the design of image restoration models also focuses on how to better design local global information processors [9, 31, 61, 63, 73]. Since the resolution of the input image is generally high in the image restoration task, directly using SA will result in a huge computation cost. To address this issue, SwinIR [31] introduced window attention [34]. HAT [9] enlarged the receptive field of the restoration transformers with the squeeze-excitation module [22] and the overlapping mechanism. Restormer [63] and DAT [10] performed channel-wise attention, thereby facilitating more efficient feature re-weighting. GRL [61] extracted the feature on local, regional, and global scales by integrating the attention of the anchor window. IPG [48] exploited the flexibility of the network by proposing the degree-variant graph solution, breaking the rigidity of the previous methods.

3. Translation Equivariance

In this section, we define the translation equivariance and propose two fundamental strategies for integrating translation equivariance into restoration networks.

Definition 3.1. Translation Equivariance. We call function $\Phi(\cdot)$ is translation equivariant to translation operation $\mathcal{T}(\cdot)$, if $\Phi(\mathcal{T}(x)) = \mathcal{T}(\Phi(x))$, where x is the input signal.

In image restoration tasks, x is an image or a feature in the latent space typically, $\mathcal{T}(\cdot)$ refers to a shift in pixels [20]. Based on this definition, two theorems are derived:

Theorem 3.2. If $\Phi(x)_i$ is transformed from $x_j = [i - b, i + b]$, where b is the sliding boundary, the function $\Phi(\cdot)$ fulfills Definition 3.1.

Theorem 3.3. If the functions $\Phi_1(\cdot)$ and $\Phi_2(\cdot)$ fulfill Definition 3.1, the functions $\Phi_2(\Phi_1(\cdot))$ and $\Phi_1(\cdot) + \Phi_2(\cdot)$ also fulfill Definition 3.1.

Reformulating the existing operators in line with Theorem 3.2 gives them the translation equivariance property. By stacking these operators, either in parallel or in serial, as specified in Theorem 3.3, more complex architectures are also capable of translation equivariance. Consequently, the model can be further enhanced via translation equivariance.

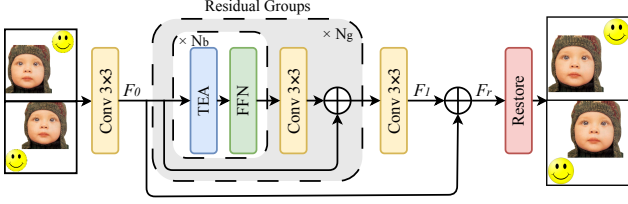


Figure 2. The overall architecture of our proposed TEAFormer.

4. Method

In this section, we conform to Theorems 3.1 and 3.2 to devise a translation equivariance restoration transformer, termed Translation Equivariance trAnsFormer (TEAFormer). We first present the overall architecture of TEAFormer and then introduce its components in detail.

4.1. Overall Architecture

The overall architecture of the proposed TEAFormer is illustrated in Figure 2 with image super-resolution (SR) presented as a demonstration. Given an input image $I \in \mathbb{R}^{H \times W \times 3}$, where $H \times W$ denotes the resolution, TEAFormer first applies a convolution layer to obtain a shallow feature $F_0 \in \mathbb{R}^{H \times W \times D}$, where D is the embedding dimension of the network. Next, following classical restoration networks [31], TEAFormer adopts a residual-in-residual structure to construct a deep feature extraction module comprised of N_g Translation Equivariance Groups (TEGs). Each TEG consists of N_b Translation Equivariance Blocks (TEBs) and a convolution layer. Each TEB, in turn, is composed of one Translation Equivariance Attention (TEA) and one feed-forward network. Subsequently, a convolutional layer is employed to extract the deep feature $F_1 \in \mathbb{R}^{H \times W \times D}$ from the feature extracted by TEGs. After extraction through the deep feature extraction module, we use the restore module to generate the high-quality image \hat{I} from the feature $F_r = F_0 + F_1$. As for other image restoration tasks that do not involve changes in resolution, we build our TEAFormer following Restormer [63].

4.2. Adaptive Translation Equivariance

Adaptive Translation Equivariance is integrated through the Adaptive Sliding Key-Value Self Attention (ASkVSA) and Downsampled Self Attention (DSA) as shown in Figure 3.

Key-value indexing in self-attention. The nature of Self Attention (SA) without position bias lies in the indexing of key-value pairs, followed by feature re-weighting. Given a flattened input $X \in \mathbb{R}^{N \times D}$, where N represents the number of tokens and D represents the embedding dimension, self-attention can be formulated as following:

$$\text{SA}(X) = \text{Softmax}\left(\frac{XW_q(XW_k)^\top}{\sqrt{D}}\right)XW_v, \quad (1)$$

where W_q , W_k , and W_v denote the weights of the linear

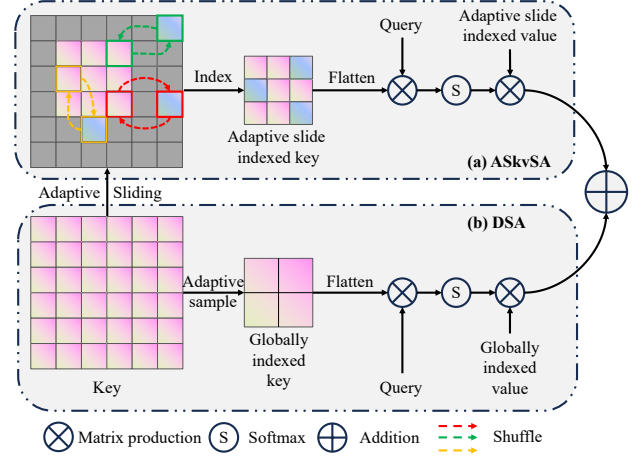


Figure 3. The inner structure of TEA with two components. (a) Adaptive Sliding key-value Self Attention (ASkVSA) and (b) Downsampled Self Attention (DSA).

projections utilized to compute the query (Q), key (K), and value (V) from input X .

In Eq. 1, the softmax similarity function is utilized for the generation of attention maps between a query and a key, while the dot product is employed for re-weighting between the attention map and a value. Given that subscripting a matrix with i returns the i -th row as a vector, an alternative equation of self-attention can be written as follows.

$$\text{SA}_i(X) = \frac{\sum_{j=1}^N \text{sim}(Q_i, K_j) V_j}{\sum_{j=1}^N \text{sim}(Q_i, K_j)}, \quad (2)$$

where $\text{sim}(Q_i, K_j) = \exp(\frac{Q_i^\top K_j}{\sqrt{D}})$.

Eq. 2 illustrates that self-attention indexes key-value pairs (K_j and V_j , $j = 1, \dots, N$) for each query (Q_i).

Sliding key-value Self Attention. In accordance with Theorem 3.2, we demonstrate that sliding window attention constitutes a generalized form of self-attention, which can be designated as Sliding Key-Value Self Attention (SkvSA). SkvSA is formulated as follows.

$$\text{SkvSA}_i(X) = \frac{\sum_{j=(i-b_1) \bmod s=0}^{(i+b_2) \bmod s=0} \text{sim}(Q_i, K_j) V_j}{\sum_{j=(i-b_1) \bmod s=0}^{(i+b_2) \bmod s=0} \text{sim}(Q_i, K_j)}, \quad (3)$$

where b_1 and b_2 are the sliding boundary on the left and right when sliding on the one-dimensional vector X . In our SkvSA, $b_1 = b_2 = \frac{w \cdot s}{2}$, where w is the size of the sliding window and s is the stride size during sliding.

Eq. 3 says that, for the i -th query Q_i , SkvSA systematically extracts the key-value pairs from a designated sliding window, extending from the index $i - \frac{w \cdot s}{2}$ to the index $i + \frac{w \cdot s}{2}$ with stride s ². Subsequently, SkvSA calculates the attention map and re-weights the feature in place.

²We set $w \cdot s \leq N$ in experiments thus enabling SkvSA to slide on X .

Boundary processing. Note that, in scenarios where $i - \frac{w \cdot s}{2} < 0$ or $i + \frac{w \cdot s}{2} > N$ occur, the slide indices of the key-value pairs j will exceed the boundary of the input X , leading to an indexing failure. To ameliorate the issue associated with slide indexing at sequence’s boundaries, we propose a boundary blocking indexing method. Specifically, for queries located at the boundary of the sequence, the slided indices of key-value pairs are “blocked” and converted into indexing within a predefined blocking window. In this study, the sizes of the predefined blocking window and the sliding window are identical. Accordingly, the sliding boundaries b can be appropriately revised as follows:

$$b = (b_1, b_2) = \begin{cases} (0, \frac{w \cdot s}{2}), & i - \frac{w \cdot s}{2} < 0, \\ (\frac{w \cdot s}{2}, N), & i + \frac{w \cdot s}{2} > N, \\ (\frac{w \cdot s}{2}, \frac{w \cdot s}{2}), & \text{others.} \end{cases} \quad (4)$$

The SkvSA and its boundary processing are capable of extracting and processing information via a fixed sliding window, adhering to the translation equivariance property as established in Theorem 3.2.

Adaptive Sliding key-value Self Attention. However, the fixed window size constrains the receptive field, leading to the entrapment of restoration transformers within rigidity [48]. To mitigate this rigidity, it is anticipated that the SkvSA will ascertain the optimal window size and position specific to each query Q_i . To achieve this endeavor, we devise the Adaptive Sliding key-value Self Attention (ASkvSA), which adaptively determines key-value indices and shuffles them within the fixed sliding window of Q_i .

As shown in Figure 3 (a), with regard to Key K and Value V , ASkvSA initially reshapes K and V from one-dimensional (1d) vectors into two-dimensional (2d) matrices. Subsequently, it applies a 2d depth-wise convolution with kernel size k to generate their adaptive indices $\mathcal{F} \in \mathbb{R}^{H \times W \times 2}$. $\mathcal{F}[h, w]$ is a vector of length 2 in the h -th row and w -th column of \mathcal{F} , which can describe a coordinate. Following this, ASkvSA performs key-value indexing based on established indices \mathcal{F}_K and \mathcal{F}_V by shuffling the pixel located at the coordinate $\mathcal{F}[h, w]$ of K and V to the pixel at the coordinate (h, w) of K and V .

$$\text{ASkvSA}(X) = \frac{\sum_{j=\mathcal{F}(K), l=\mathcal{F}(V)} \text{sim}(Q_i, K_j) V_l}{\sum_{j=\mathcal{F}(K)} \text{sim}(Q_i, K_j)}. \quad (5)$$

Adaptive slide indexing does not compromise the translation equivariance of ASkvSA. ASkvSA stacks convolutions with SkvSA in serial to generate adaptive indices of key-value pairs. Given that convolution satisfies the property of translation equivariance, when $K_{h,w}$ is translated to $K_{h+\delta_h, w+\delta_w}$, key’s adaptive indices \mathcal{F}_K will shuffle the pixel located at $\mathcal{F}[h+\delta_h, w+\delta_w]$ of K to the pixel at $(h+\delta_h, w+\delta_w)$ of K . According to Theorem 3.3, ASkvSA satisfies the translation equivariance property.

Adaptively aggregated with global key-value pairs. Although ASkvSA can identify appropriate key-value pairs beyond a fixed sliding window, some remote but valid pixels still escape ASkvSA’s indexing. Consequently, we propose downsampled self-attention (DSA), which adaptively combines global key value indexes through downsampling, providing the network with a coarse, yet efficient global indexing of key-value pairs. DSA can be formulated as:

$$\text{DSA}_i(X) = \frac{\sum_{j=1}^{N_d} \text{sim}(Q_i, K'_j) V'_j}{\sum_{j=1}^{N_d} \text{sim}(Q_i, K'_j)}, \quad (6)$$

where K' and V' represents the downsampled key-value pair calculated in ASkvSA, and N_d denotes the number of tokens associated with the downsampled key-value pair. We employ average pooling as the downsampling operator due to its efficiency and coarse fulfillment³ of TE.

Finally, according to Figure 3, the ASkvSA and DSA outputs are adaptively aggregated to obtain our TEA.

$$\text{TEA}_i(X) = \alpha_s \text{ASkvSA}(X) + \alpha_d \text{DSA}(X), \quad (7)$$

where α_s and α_d are learnable parameters. TEA stacks DSA with ASkvSA in parallel. According to Theorem 3.3, TEA satisfies the translation equivariance property.

4.3. Computational Cost and Hyper-Parameters

We demonstrate that TEA can maintain a computational cost that is similar to that of window attention [34] under well-designed hyperparameter settings. We first list four integral hyperparameters of TEA:

- w : the sliding window size of ASkvSA;
- s : the sliding stride size of ASkvSA;
- k : the kernel size of adaptive indexes generation;
- N_d : the number of tokens in DSA.

According to Section 4.2, TEA uses $3ND^2$ FLOPs for the Query-Key-Value linear projections, $2NDk^2$ FLOPs for the depth-wise convolution in adaptive indices generation, Nw^2D FLOPs for attention map computation between query $Q \in \mathbb{R}^{N \times D}$ and indexed key $K \in \mathbb{R}^{w^2 \times D}$, Nw^2D FLOPs for feature re-weighting between attention map and indexed value $V \in \mathbb{R}^{w^2 \times D}$, and $2NN_dD$ FLOPs for DSA. The total FLOPs of TEA is $3ND^2 + 2NDk^2 + 2Nw^2D + 2NN_dD$. With the hyper-parameters held constant, the FLOPs of TEA exhibit linear growth as a function of N , thereby implying that TEA is $\mathcal{O}(N)$.

Consequently, when the hyper-parameters of TEA are adjusted carefully, its computational cost becomes comparable to that of window attention. In our TEAFormer, the hyper-parameter w has been set to 15, k to 3, and N_d to 16, thereby modulating the computational complexity of TEA to be even slightly lower than that of window attention with window size 16.

³ [45] proved that downsampling can meet strict TE through learnable polyphase (LP). We compare these downsamplers in Sec. 5.6

Model	window size	Translation equivariance			Params	FLOPs	Latency	Performance	NTK [25]	SRGA [33]
		SkvSA	ASkvSA	DSA	(M)	(T)	(ms)	Urban100 [24] PSNR↑ / SSIM↑	Condition ↓	Value ↓
SwinIR [31]	8				11.90	0.462	130.0	27.45 / 0.8254	1746.49	3.655
SwinIR-Large	16				21.42	0.897	214.5	27.94 / 0.8362	1554.65	3.610
TEAFormer	15	✓			21.86	0.688	230.1	28.31 / 0.8444	243.75	3.206
TEAFormer	15		✓		21.98	0.757	284.4	28.47 / 0.8457	283.99	3.298
TEAFormer	15	✓		✓	21.86	0.966	340.9	28.49 / 0.8470	203.06	3.261
TEAFormer	15		✓	✓	21.98	1.035	386.7	28.67 / 0.8489	236.78	3.275

Table 2. Ablation study on TEA. Our TEA enhances performance, convergence speed, and generalization.

Method	Scale	Params (M)	FLOPs (T)	Latency (ms)	Set5 [5]		Set14 [64]		B100 [37]		Urban100 [24]		Manga109 [40]	
					PSNR ↑	SSIM ↑	PSNR ↑	SSIM ↑	PSNR ↑	SSIM ↑	PSNR ↑	SSIM ↑	PSNR ↑	SSIM ↑
EDSR [32]	×2	40.7	6.006	147.1	38.11	0.9602	33.92	0.9195	32.32	0.9013	32.93	0.9351	39.10	0.9773
RCAN [71]		15.4	2.259	155.5	38.27	0.9614	34.12	0.9216	32.41	0.9027	33.34	0.9384	39.44	0.9786
SwinIR-L [31]		0.91	156.4	188.6	38.14	0.9611	33.86	0.9206	32.31	0.9012	32.76	0.9340	39.12	0.9783
SwinIR [31]		11.8	1.848	514.4	38.42	0.9623	34.46	0.9250	32.53	0.9041	33.81	0.9427	39.92	0.9797
EDT [30]		11.5	1.965	1010	38.45	0.9624	34.57	0.9258	32.52	0.9041	33.80	0.9425	39.93	0.9800
SRFormer [73]		10.3	1.790	787.2	38.51	0.9627	34.44	0.9253	32.57	0.9046	34.09	0.9449	40.07	0.9802
HAT [9]		20.6	3.662	901.9	38.63	0.9630	34.86	0.9274	32.62	0.9053	34.45	0.9466	40.26	0.9809
GRL-B* [61]		20.1	4.422	2621	38.48	0.9627	34.64	0.9265	32.55	0.9045	33.97	0.9437	40.06	0.9804
DAT [10]		14.7	2.155	1215	38.58	0.9629	34.81	0.9272	32.61	0.9051	34.37	0.9458	40.33	0.9807
IPG [48]		16.8	4.732	2703	38.61	0.9632	34.73	0.9270	32.60	0.9052	34.48	0.9464	40.24	0.9810
TEAFormer-L (Ours)		0.83	0.237	254.0	38.27	0.8618	34.26	0.9240	32.43	0.9029	33.51	0.9396	39.56	0.9792
TEAFormer (Ours)		21.8	4.133	1493	38.64	0.9631	35.12	0.9284	32.72	0.9064	35.23	0.9509	40.32	0.9807
EDSR [32]	×4	43.1	1.853	49.13	32.46	0.8968	28.80	0.7876	27.71	0.7420	26.64	0.8033	31.02	0.9148
RCAN [71]		15.6	0.587	46.15	32.63	0.9002	28.87	0.7889	27.77	0.7436	26.82	0.8087	31.22	0.9173
SwinIR-L [31]		0.88	0.039	48.71	32.44	0.8976	28.77	0.7858	27.69	0.7406	26.47	0.7980	30.92	0.9151
SwinIR [31]		11.9	0.462	130.0	32.92	0.9044	29.09	0.7950	27.92	0.7489	27.45	0.8254	32.03	0.9260
EDT [30]		11.6	0.514	251.3	32.82	0.9031	29.09	0.7939	27.91	0.7483	27.46	0.8246	32.03	0.9254
SRFormer [73]		10.4	0.470	189.2	32.93	0.9041	29.08	0.7953	27.94	0.7502	27.68	0.8311	32.44	0.9271
HAT [9]		20.8	0.938	227.7	33.04	0.9056	29.23	0.7973	28.00	0.7517	27.97	0.8368	32.48	0.9292
GRL-B* [61]		20.2	1.129	761.8	32.90	0.9039	29.14	0.7956	27.96	0.7497	27.53	0.8276	32.19	0.9266
DAT [10]		14.8	0.561	296.8	33.08	0.9055	29.23	0.7973	28.00	0.7515	27.87	0.8343	32.51	0.9291
IPG [48]		17.0	1.206	646.7	33.15	0.9062	29.24	0.7973	27.99	0.7519	28.13	0.8392	32.53	0.9300
TEAFormer-L (Ours)		0.83	0.059	69.64	32.63	0.9002	28.96	0.7899	27.82	0.7442	27.04	0.8105	31.56	0.9197
TEAFormer (Ours)		22.0	1.035	386.7	33.23	0.9066	29.46	0.8009	28.11	0.7544	28.67	0.8489	32.99	0.9323

Table 3. *Classical image SR* results. Performance and complexity are shown for better comparison. Dash lines separate the results of CNNs and Transformers. The best two scores in each column are highlighted in red and blue. Methods with “*” are replicated with standard training setting, following IPG [48]. The “-L” indicates that the given method is a lightweight version.

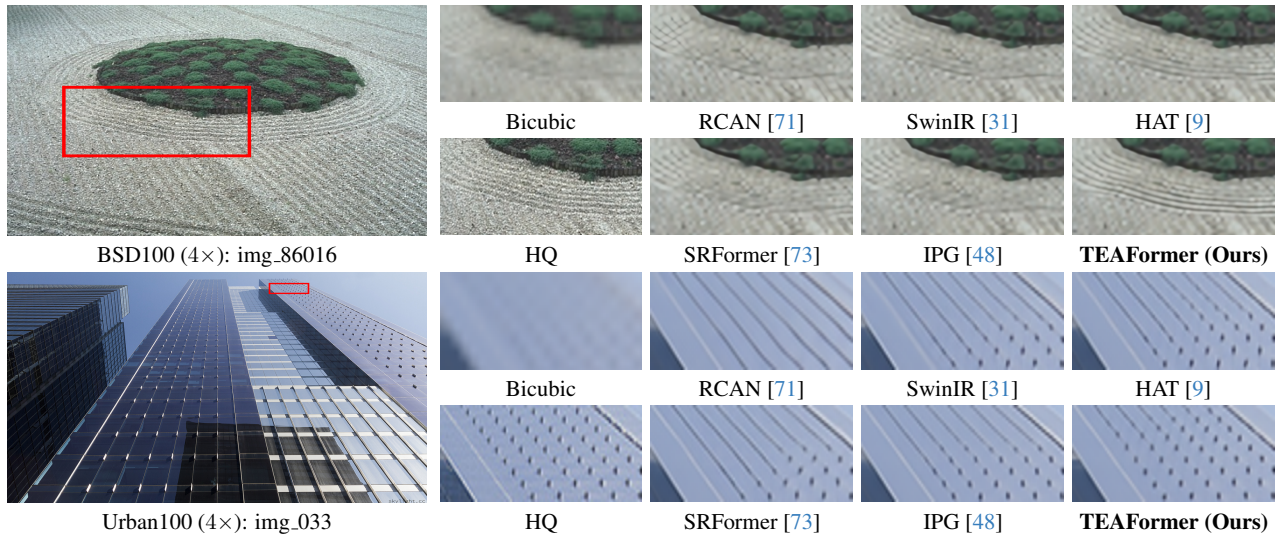


Figure 4. Qualitative comparison with recent SOTA methods on the *image SR* task.

Method	Params	Indoor Scenes				Outdoor Scenes				Combined			
	(M)	PSNR \uparrow	SSIM \uparrow	MAE \downarrow	LPIPS \downarrow	PSNR \uparrow	SSIM \uparrow	MAE \downarrow	LPIPS \downarrow	PSNR \uparrow	SSIM \uparrow	MAE \downarrow	LPIPS \downarrow
DPDNet _S [1]	32.3	26.54	0.816	0.031	0.239	22.25	0.682	0.056	0.313	24.34	0.747	0.044	0.277
KPAC _S [47]	2.06	27.97	0.852	0.026	0.182	22.62	0.701	0.053	0.269	25.22	0.774	0.040	0.227
IFAN _S [27]	10.5	28.11	0.861	0.026	0.179	22.76	0.720	0.052	0.254	25.37	0.789	0.039	0.217
Restormer _S [63]	26.1	28.87	0.882	0.025	0.145	23.24	0.743	0.050	0.209	25.98	0.811	0.038	0.178
SFNet _S [12]	13.2	29.16	0.878	0.023	0.168	23.45	0.747	0.049	0.244	26.23	0.811	0.037	0.207
GRL _S -B [61]	19.9	29.06	0.886	0.024	0.139	23.45	0.761	0.049	0.196	26.18	0.822	0.037	0.168
IRNeXT _S [13]	13.2	29.22	0.879	0.024	0.167	23.53	0.752	0.049	0.244	26.30	0.814	0.037	0.206
TEAFormer _S (Ours)	15.4	29.50	0.892	0.023	0.150	23.55	0.767	0.050	0.211	26.45	0.828	0.037	0.181
DPDNet _D [1]	32.3	27.48	0.849	0.029	0.189	22.90	0.726	0.052	0.255	25.13	0.786	0.041	0.223
RDPD _D [2]	8.20	28.10	0.843	0.027	0.210	22.82	0.704	0.053	0.298	25.39	0.772	0.040	0.255
IFAN _D [27]	10.5	28.66	0.868	0.025	0.172	23.46	0.743	0.049	0.240	25.99	0.804	0.037	0.207
Restormer _D [63]	26.1	29.48	0.895	0.023	0.134	23.97	0.773	0.047	0.175	26.66	0.833	0.035	0.155
Uformer _D [54]	20.6	28.23	0.860	0.026	0.199	23.10	0.728	0.051	0.285	25.65	0.795	0.039	0.243
GRL _D -B [61]	19.9	29.83	0.903	0.022	0.114	24.39	0.795	0.045	0.150	27.04	0.847	0.034	0.133
TEAFormer _D (Ours)	15.4	30.16	0.905	0.022	0.128	24.45	0.795	0.045	0.170	27.23	0.849	0.034	0.150

Table 4. *Defocus deblurring* comparisons on the DPDD [1] testset (containing 37 indoor and 39 outdoor scenes). **S**: single-image defocus deblurring. **D**: dual-pixel defocus deblurring. The best two results are highlighted in red and blue, respectively.

5. Experiments

5.1. Ablation study

We analyze the influence exerted by the TEA on both performance, computational complexity, generalization, and training convergence in Table 2. In this experiment, we disassemble TEA into several plug-and-play modules and gradually add them into the SwinIR baseline restoration network. To ensure comparable parameters and FLOPs among the models being evaluated, we adjusted the window size of SwinIR to 16 and increased the number of parameters to 21 M, which is termed **SwinIR-Large**. Following the incorporation of our SkvSA, there is a marked improvement in the convergence rate and generalization abilities. Subsequent to the integration of our ASkvSA and DSA, there is a progressive enhancement in the model’s performance, without detrimental effects on convergence and generalization. The results of this experiment demonstrate the efficacy of each component within the TEA. Furthermore, it illustrates that TEA resolves the dilemma between self-attention and sliding window attention, thereby attaining high performance by the global receptive field and reducing computational complexity simultaneously.

5.2. Image SR

Training settings. We used the same training hyperparameters and evaluation methods as IPG [48]. All of our models were trained from scratch on the DF2K [3, 32] datasets with 64×64 resolution. The optimizer was Adam [26], the learning rate was 2×10^{-4} while using the cosine scheduler. We used L_1 loss as a criterion.

Results. We first compare TEAFormer with various classical image SR methods, including EDSR [32], RCAN [71], SwinIR [31], EDT [30], HAT [9], SRFormer [73], GRL [61], DAT [10], and IPG [48]. We compare them on synthetic benchmarks [5, 24, 37, 40, 64] generated by bicubic downsampling. The FLOPs and latency reported were

calculated with one NVIDIA A800 GPU on 768 resolution.

The quantitative comparison of the methods for classical image SR is shown in Table 3. The exceptional performance of TEAFormer is distinctly evident as it achieves the highest results across nearly all five datasets for various scale factors. Incorporating the attention module with translation equivalence introduces a more suitable and productive inductive bias to the restoration model, thereby enhancing its performance. For the $\times 4$ SR, our TEAFormer achieves a 28.67 dB PSNR score on the Urban100 dataset, which is 0.7 dB higher than HAT [9] while both has 20M parameters. In comparison to the preceding image SR method IPG [48], TEAFormer demonstrates a gain of 0.54 dB with comparable FLOPs and a $2\times$ faster inference.

We further conduct TEAFormer-Light, which only comprises 829k parameters. In comparison to the CNN method HAN [42], TEAFormer-Light has been demonstrated to achieve superior performance with only its 1.3% parameters. In comparison to other lightweight transformer methods, TEAFormer also demonstrates an absolute performance advantage, as evidenced by the fact that TEAFormer-Light achieves a higher PSNR than SwinIR-L on the Urban100 [24] dataset by 0.57 dB.

5.3. Image Defocus Deblurring

Training settings. We employed the same training hyperparameters and evaluation as Restormer [63] in image deblurring tasks. Our TEAFormer were trained from scratch using progressive learning [63]. During the training phase, the optimizer adopted was AdamW [35] with L_1 loss.

Results. We compare our TEAFormer with single image defocus deblurring methods [1, 13, 14, 27, 47, 61, 63] and dual-pixel image defocus deblurring methods [1, 2, 27, 54, 61, 63] on DPDD [1] dataset in Table 4. Our TEAFormer significantly outperforms state-of-the-art schemes for the single-image and dual-pixel defocus deblurring tasks on PSNR and SSIM metrics. In particular in the category

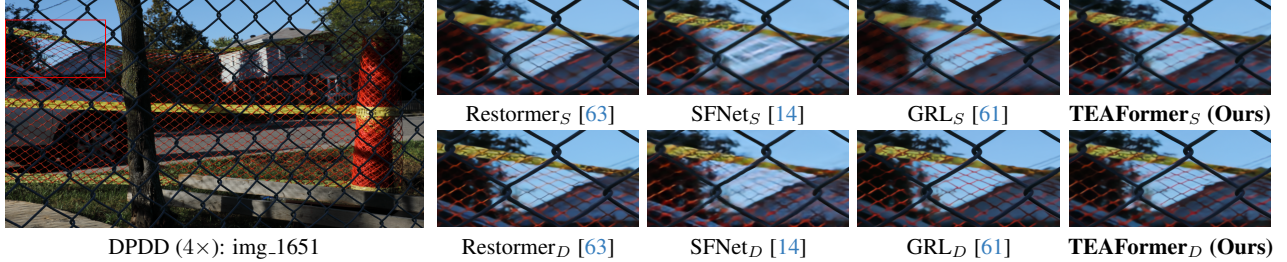


Figure 5. Qualitative comparison with recent SOTA methods on the *image defocus blur* task. Please zoom in for better view.

Method	Params	Color												Grayscale								
		CBSD68 [39]			Kodak24 [17]			McMaster [69]			Urban100 [24]			Set12 [67]			BSD68 [39]			Urban100 [24]		
	(M)	$\sigma=15$	$\sigma=25$	$\sigma=50$	$\sigma=15$	$\sigma=25$	$\sigma=50$	$\sigma=15$	$\sigma=25$	$\sigma=50$	$\sigma=15$	$\sigma=25$	$\sigma=50$	$\sigma=15$	$\sigma=25$	$\sigma=50$	$\sigma=15$	$\sigma=25$	$\sigma=50$	$\sigma=15$	$\sigma=25$	$\sigma=50$
DnCNN [67]	0.56	33.90	31.24	27.95	34.60	32.14	28.95	33.45	31.52	28.62	32.98	30.81	27.59	32.86	30.44	27.18	31.73	29.23	26.23	32.64	29.95	26.26
DRUNet [68]	32.6	34.30	31.69	28.51	35.31	32.89	29.86	35.40	33.14	30.08	34.81	32.60	29.61	33.25	30.94	27.90	31.91	29.48	26.59	33.44	31.11	27.96
EDT-B [30]	11.5	34.39	31.76	28.56	35.37	32.94	29.87	35.61	33.34	30.25	35.22	33.07	30.16	-	-	-	-	-	-	-	-	-
SwinIR* [31]	11.7	34.39	31.78	28.55	35.33	32.88	29.77	35.59	33.20	30.19	35.11	32.89	29.77	33.34	31.00	27.88	31.96	29.49	26.58	33.61	31.20	27.86
Restormer [63]	26.1	34.39	31.78	28.59	35.44	33.02	30.00	35.55	33.31	30.29	35.06	32.91	30.02	33.35	31.04	28.01	31.95	29.51	26.62	33.67	31.39	28.33
ART* [66]	16.2	34.40	31.79	28.59	35.47	33.04	30.00	35.61	33.33	30.27	35.12	32.95	29.99	33.35	31.05	28.01	31.95	29.50	26.59	33.71	31.47	28.40
GRL-B* [61]	19.8	34.40	31.78	28.58	35.42	33.03	30.02	35.63	33.36	30.26	35.22	33.01	30.24	33.34	31.02	27.99	31.95	29.50	26.60	33.73	31.54	28.49
TEAFormer (Ours)	15.4	34.40	31.80	28.62	35.50	33.08	30.05	35.68	33.42	30.38	35.25	33.18	30.37	33.37	31.06	28.04	31.96	29.52	26.63	33.89	31.65	28.61

Table 5. *Color and grayscale image Gaussian denoising* results in terms of PSNR \uparrow . Model complexity and prediction accuracy are shown for better comparison. Dash lines separate the results of CNNs and Transformers. The best two results are highlighted in **red** and **blue**, respectively. Methods with “*” are replicated with standard training setting, which learns a single model to handle various noise levels.

of single-pixel indoor scene, TEAFormer yields 0.44 dB improvements over the GRL previous best transformer method [61]. Figure 5 illustrates that our TEAFormer is more effective in removing spatially varying defocus blur than other restoration transformers.

5.4. Image Denoising

Training settings. The image denoising and defocus deblurring tasks used the same hyper-parameters for training.

Gaussian Denoising Results. We perform denoising experiments on synthetic benchmark datasets generated with additive white Gaussian noise (Set12 [67], BSD68 [38], Urban100 [24], Kodak24 [17] and McMaster [69]). Following DRUNet [68], we learn a single model to handle various noise levels, including 15, 25, and 50. Our TEAFormer achieves state-of-the-art performance under both experimental settings on different datasets and noise levels. Specifically, for the challenging noise level 50 on color Urban100 [24] dataset, TEAFormer achieves 0.13 dB gain over the previous best restoration transformer GRL [61], as shown in Table 5. Similar performance gains can be observed for the Gaussian gray denoising.

5.5. All-in-one Image Restoration

Training settings. Following DCPT [23], a 5D all-in-one image restoration and enhancement task was conducted with the objective of training the network to eliminate five distinct types of degradation: haze, rain, Gaussian noise, motion blur, and low light. The models were trained from scratch on datasets with 128×128 resolution without progressive learning. During training, the optimizer was set as AdamW, the learning rate was set as 3×10^{-4} while using

the cosine scheduler. We used L_1 loss as a criterion.

Results. As illustrated in Table 6, TEAFormer surpasses the most recently proposed methods specifically designed for comprehensive all-in-one restoration tasks (IDR [65], PromptIR [43], and InstructIR [11]). The average PSNR of TEAFormer in all five tasks reached 31.22 dB, thereby exceeding the current state-of-the-art 5D all-in-one restoration method, InstructIR [11], by 1.67 dB. TEAFormer consistently outperforms prior PSNR in every indicator of each task, signifying its exceptional proficiency in image restoration under complex multi-task conditions.

Mixed degradation. As shown in Table 7, TEAFormer surpasses the most recently proposed methods under mixed degradation scenarios, specifically designed for universal restoration tasks [36, 72]). Within scenarios characterized by a combination of three degradation (low-light, haze, and rain), TEAFormer demonstrates superior performance over the current state-of-the-art universal restoration method, DiffUIR [72], by a margin of 0.42 dB.

5.6. Discussion

Hyperparameters analysis. The performance under various hyperparameters is reported in Table 8 (w), Table 9 (s), Table 10 (k) and Table 11 (N_d). Our settings ($w = 15$, $s = 4$, $k = 3$, $N_d = 16$) optimally balanced performance and computation cost. Note that changing some of the hyperparameters does not affect the computational complexity as discussed in Section 4.3. For s in Table 9, parameters and FLOPs are omitted because s does not affect them.

Compare different downsampler in DSA. The incorporation of DSA into our TEA substantially enhances the performance of the model without adding undue complexity.

Method	Params	Dehazing on SOTS [28]	Deraining on Rain100L [60]	Denoising on BSD68 [38]	Deblurring on GoPro [41]	Low-Light on LOL [55]	Average
	(M)	PSNR↑ / SSIM↑	PSNR↑ / SSIM↑	PSNR↑ / SSIM↑	PSNR↑ / SSIM↑	PSNR↑ / SSIM↑	PSNR↑ / SSIM↑
AirNet [29]	8.90	21.04 / 0.884	32.98 / 0.951	30.91 / 0.882	24.35 / 0.781	18.18 / 0.735	25.49 / 0.846
IDR [65]	15.3	25.24 / 0.943	35.63 / 0.965	31.60 / 0.887	27.87 / 0.846	21.34 / 0.826	28.34 / 0.893
PromptIR [43]	35.6	25.20 / 0.931	35.94 / 0.964	31.17 / 0.882	27.32 / 0.842	20.94 / 0.799	28.11 / 0.883
InstructIR [11]	35.1	27.10 / 0.956	36.84 / 0.973	31.40 / 0.887	29.40 / 0.886	23.00 / 0.836	29.55 / 0.907
<hr/>							
SwinIR [31]	11.8	21.50 / 0.891	30.78 / 0.923	30.59 / 0.868	24.52 / 0.773	17.81 / 0.723	25.04 / 0.835
NAFNet [7]	67.9	25.23 / 0.939	35.56 / 0.967	31.02 / 0.883	26.53 / 0.808	20.49 / 0.809	27.76 / 0.881
Restormer [63]	26.1	24.09 / 0.927	34.81 / 0.962	31.49 / 0.884	27.22 / 0.829	20.41 / 0.806	27.60 / 0.881
TEAFormer (Ours)	15.4	31.57 / 0.980	39.44 / 0.986	31.54 / 0.890	30.53 / 0.908	23.06 / 0.856	31.22 / 0.924

Table 6. **5D All-in-one image restoration results.** Dash lines separate the results of methods designed specifically for all-in-one image restoration task and methods that only focus on architecture enhancement. The best two results are highlighted in red and blue, respectively. TEAFormer sets the new state-of-the-art performance in each task.

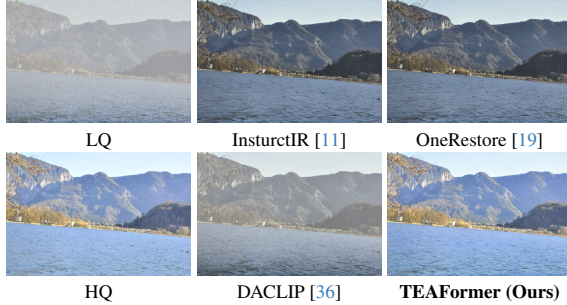


Figure 6. **Visual comparison on low-light+haze+rain mixed degradation.** TEAFormer can restore the correct lightness.

Method	Params low-light+haze+rain low-light+haze+snow		
	(M)	PSNR↑ / SSIM↑	PSNR↑ / SSIM↑
AirNet [29]	8.90	21.80 / 0.708	22.23 / 0.725
TransWeather [50]	31.0	21.55 / 0.678	21.01 / 0.655
PromptIR [43]	35.6	23.74 / 0.752	23.33 / 0.747
DACLIP [36]	174	22.96 / 0.712	23.32 / 0.751
DiffUIR-L [72]	36.3	25.46 / 0.779	25.89 / 0.788
OneRestore [19]	5.98	25.18 / 0.795	25.28 / 0.797
InstructIR [11]	35.1	24.84 / 0.777	24.32 / 0.760
TEAFormer (Ours)	15.4	25.88 / 0.796	26.05 / 0.800

Table 7. **Mixed degraded image restoration results on CDD [19].**

w	FLOPs	Urban100 [24]	s	FLOPs	Urban100 [24]	k	FLOPs	Urban100 [24]	N_d	FLOPs	Urban100 [24]	Down	S-conv	Urban100 [24]
	(T)	PSNR \uparrow / SSIM \uparrow		PSNR \uparrow / SSIM \uparrow	(T)		PSNR \uparrow / SSIM \uparrow	(T)		PSNR \uparrow / SSIM \uparrow	(%) \uparrow		PSNR \uparrow / SSIM \uparrow	
7	0.827	28.35 / 0.8441	1	28.43 / 0.8431	None	0.966	28.49 / 0.8470	None	0.757	28.47 / 0.8457	MaxPool	87.3	28.61 / 0.8477	
15	1.035	28.67 / 0.8489	2	28.51 / 0.8453	1	1.028	28.53 / 0.8471	16	1.035	28.67 / 0.8489	LPD	91.7	28.64 / 0.8493	
31	1.866	28.73 / 0.8493	4	28.67 / 0.8489	3	1.035	28.67 / 0.8489	N	18.36	28.80 / 0.8503	AvgPool	91.2	28.67 / 0.8489	

Table 8. Ablations of sliding window size w .

Table 9. Ablations of sliding stride s .

Table 10. Ablations of kernel size k for adaptive indices. “None” stands for no adaptive indices used.

Table 11. Ablations of N_d in DSA. “None” stands for no DSA used.

Table 12. Ablations of downsamplers in DSA. The higher the S-Conv, the more strictly the model meets TE.

However, the average pooling employed in DSA does not strictly adhere to the property of TE. Using a comparative ablation of several downsampling modules in Table 12, we experimentally demonstrate that the use of average pooling does not compromise the model’s performance or its TE.

Does TEAFormer converge faster and generalize better in practice? Table 1 and Table 2 have illustrated that TEAFormer converges faster and generalizes better than other networks theoretically due to the incorporation of translation equivariance. Figure 7 (left) further demonstrates that TEAFormer reaches a lower loss faster than other restoration transformers [9, 31] in practice. Following MaskDenoise [6], we compare the statistics of the last layer feature in SwinIR [31] and TEAFormer under two different real-world degradations on the PIES [33] dataset (out of the training dataset) in Figure 7 (right). The results show that TEAFormer can produce a more consistent output when processing LQ images with different degradations. Therefore, TEAFormer generalizes better in practice.

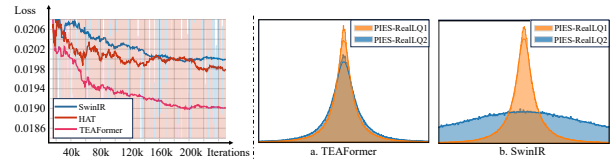


Figure 7. Comparison on convergence (left) and generalization (right).

6. Conclusion

In this paper, we start by examining the translation equivariance, which serves as an inherent inductive bias in image restoration. We then define the translation equivariance and offer two strategies for incorporating it into restoration networks: (1) slide indexing and (2) component stacking. To address the fixed receptive field provided by these strategies, we proposed TEA and TEAFormer via adaptive key-value indexing. The efficacy of TEAFormer has been demonstrated in various image restoration tasks, with ablation studies confirming that this efficacy arises from the incorporation of TEA. In the future, we intend to explore more equivariances into restoration networks.

Acknowledgement

This work was supported financially the Natural Science Foundation of China (82371112, 623B2001), the Science Foundation of Peking University Cancer Hospital (JC202505), Natural Science Foundation of Beijing Municipality (Z210008) and the Clinical Medicine Plus X - Young Scholars Project of Peking University, the Fundamental Research Funds for the Central Universities (PKU2025PKULCXQ008).

References

- [1] Abdullah Abuolaim and Michael S Brown. Defocus deblurring using dual-pixel data. In *European Conference on Computer Vision*, pages 111–126. Springer, 2020. 6
- [2] Abdullah Abuolaim, Mauricio Delbracio, Damien Kelly, Michael S Brown, and Peyman Milanfar. Learning to reduce defocus blur by realistically modeling dual-pixel data. In *Proceedings of the IEEE/CVF International Conference on Computer Vision (ICCV)*, 2021. 6
- [3] Eirikur Agustsson and Radu Timofte. Ntire 2017 challenge on single image super-resolution: Dataset and study. In *The IEEE Conference on Computer Vision and Pattern Recognition (CVPR) Workshops*, 2017. 6
- [4] Irwan Bello, Barret Zoph, Ashish Vaswani, Jonathon Shlens, and Quoc V Le. Attention augmented convolutional networks. In *Proceedings of the IEEE/CVF international conference on computer vision*, pages 3286–3295, 2019. 2
- [5] Marco Bevilacqua, Aline Roumy, Christine Guillemot, and Marie Line Alberi-Morel. Low-complexity single-image super-resolution based on nonnegative neighbor embedding. In *British Machine Vision Conference*. BMVA press, 2012. 5, 6
- [6] Haoyu Chen, Jinjin Gu, Yihao Liu, Salma Abdel Magid, Chao Dong, Qiong Wang, Hanspeter Pfister, and Lei Zhu. Masked image training for generalizable deep image denoising. In *Proceedings of the IEEE/CVF Conference on Computer Vision and Pattern Recognition*, pages 1692–1703, 2023. 8
- [7] Liangyu Chen, Xiaojie Chu, Xiangyu Zhang, and Jian Sun. Simple baselines for image restoration. In *Computer Vision – ECCV 2022*, pages 17–33, Cham, 2022. Springer Nature Switzerland. 8
- [8] Xiangning Chen, Cho-Jui Hsieh, and Boqing Gong. When vision transformers outperform resnets without pre-training or strong data augmentations. In *International Conference on Learning Representations*, 2022. 1
- [9] Xiangyu Chen, Xintao Wang, Jiantao Zhou, Yu Qiao, and Chao Dong. Activating more pixels in image super-resolution transformer. In *Proceedings of the IEEE/CVF Conference on Computer Vision and Pattern Recognition (CVPR)*, pages 22367–22377, 2023. 2, 5, 6, 8
- [10] Zheng Chen, Yulun Zhang, Jinjin Gu, Linghe Kong, Xiaokang Yang, and Fisher Yu. Dual aggregation transformer for image super-resolution. In *ICCV*, 2023. 2, 5, 6
- [11] Marcos V Conde, Gregor Geigle, and Radu Timofte. Instructir: High-quality image restoration following human instructions. In *Proceedings of the European Conference on Computer Vision (ECCV)*, 2024. 7, 8
- [12] Yuning Cui, Yi Tao, Zhenshan Bing, Wenqi Ren, Xinwei Gao, Xiaochun Cao, Kai Huang, and Alois Knoll. Selective frequency network for image restoration. In *The Eleventh International Conference on Learning Representations*, 2022. 6
- [13] Yuning Cui, Wenqi Ren, Sining Yang, Xiaochun Cao, and Alois Knoll. Innext: Rethinking convolutional network design for image restoration. In *Proceedings of the 40th International Conference on Machine Learning*, 2023. 6
- [14] Yuning Cui, Yi Tao, Zhenshan Bing, Wenqi Ren, Xinwei Gao, Xiaochun Cao, Kai Huang, and Alois Knoll. Selective frequency network for image restoration. In *The Eleventh International Conference on Learning Representations*, 2023. 6, 7
- [15] Xiaoyi Dong, Jianmin Bao, Dongdong Chen, Weiming Zhang, Nenghai Yu, Lu Yuan, Dong Chen, and Baining Guo. Cswin transformer: A general vision transformer backbone with cross-shaped windows. In *Proceedings of the IEEE/CVF conference on computer vision and pattern recognition*, pages 12124–12134, 2022. 2
- [16] Alexey Dosovitskiy, Lucas Beyer, Alexander Kolesnikov, Dirk Weissenborn, Xiaohua Zhai, Thomas Unterthiner, Mostafa Dehghani, Matthias Minderer, Georg Heigold, Sylvain Gelly, Jakob Uszkoreit, and Neil Houlsby. An image is worth 16x16 words: Transformers for image recognition at scale. In *International Conference on Learning Representations*, 2021. 2
- [17] Rich Franzen. Kodak lossless true color image suite, 2013. 7
- [18] Jonathan Gordon, Wessel P. Bruinsma, Andrew Y. K. Foong, James Requeima, Yann Dubois, and Richard E. Turner. Convolutional conditional neural processes. In *International Conference on Learning Representations*, 2020. 1
- [19] Yu Guo, Yuan Gao, Yuxu Lu, Ryan Wen Liu, and Shengfeng He. Onerestore: A universal restoration framework for composite degradation. In *European Conference on Computer Vision*, 2024. 8
- [20] Ali Hassani, Steven Walton, Jiachen Li, Shen Li, and Humphrey Shi. Neighborhood attention transformer. In *Proceedings of the IEEE/CVF Conference on Computer Vision and Pattern Recognition*, pages 6185–6194, 2023. 2
- [21] Ali Hatamizadeh, Greg Heinrich, Hongxu Yin, Andrew Tao, Jose M Alvarez, Jan Kautz, and Pavlo Molchanov. Fastervit: Fast vision transformers with hierarchical attention. In *The Twelfth International Conference on Learning Representations*, 2024. 2
- [22] Jie Hu, Li Shen, and Gang Sun. Squeeze-and-excitation networks. In *Proceedings of the IEEE conference on computer vision and pattern recognition*, pages 7132–7141, 2018. 2
- [23] JiaKui Hu, Lujia Jin, Zhengjian Yao, and Yanye Lu. Universal image restoration pre-training via degradation classification. *The Thirteenth International Conference on Learning Representations*, 2025. 7

- [24] Jia-Bin Huang, Abhishek Singh, and Narendra Ahuja. Single image super-resolution from transformed self-exemplars. In *2015 IEEE Conference on Computer Vision and Pattern Recognition (CVPR)*, pages 5197–5206, 2015. 5, 6, 7, 8
- [25] Arthur Jacot, Franck Gabriel, and Clément Hongler. Neural tangent kernel: Convergence and generalization in neural networks. *Advances in neural information processing systems*, 31, 2018. 1, 5
- [26] Diederik Kingma and Jimmy Ba. Adam: A method for stochastic optimization. In *International Conference on Learning Representations (ICLR)*, San Diego, CA, USA, 2015. 6
- [27] Junyong Lee, Hyeonseok Son, Jaesung Rim, Sunghyun Cho, and Seungyong Lee. Iterative filter adaptive network for single image defocus deblurring. In *Proceedings of the IEEE Conference on Computer Vision and Pattern Recognition (CVPR)*, 2021. 6
- [28] Boyi Li, Wenqi Ren, Dengpan Fu, Dacheng Tao, Dan Feng, Wenjun Zeng, and Zhangyang Wang. Benchmarking single-image dehazing and beyond. *TIP*, 2018. 8
- [29] Boyun Li, Xiao Liu, Peng Hu, Zhongqin Wu, Jiancheng Lv, and Xi Peng. All-in-one image restoration for unknown corruption. In *CVPR*, 2022. 8
- [30] Wenbo Li, Xin Lu, Shengju Qian, and Jiangbo Lu. On efficient transformer-based image pre-training for low-level vision. In *Proceedings of the Thirty-Second International Joint Conference on Artificial Intelligence, IJCAI-23*, pages 1089–1097. International Joint Conferences on Artificial Intelligence Organization, 2023. Main Track. 5, 6, 7
- [31] Jingyun Liang, Jiezhong Cao, Guolei Sun, Kai Zhang, Luc Van Gool, and Radu Timofte. Swinir: Image restoration using swin transformer. In *Proceedings of the IEEE/CVF international conference on computer vision*, pages 1833–1844, 2021. 2, 3, 5, 6, 7, 8
- [32] Bee Lim, Sanghyun Son, Heewon Kim, Seungjun Nah, and Kyoung Mu Lee. Enhanced deep residual networks for single image super-resolution. In *Proceedings of the IEEE conference on computer vision and pattern recognition workshops*, pages 136–144, 2017. 1, 5, 6
- [33] Yihao Liu, Hengyuan Zhao, Jinjin Gu, Yu Qiao, and Chao Dong. Evaluating the generalization ability of super-resolution networks. *IEEE Transactions on Pattern Analysis and Machine Intelligence*, 45(12):14497–14513, 2023. 1, 5, 8
- [34] Ze Liu, Yutong Lin, Yue Cao, Han Hu, Yixuan Wei, Zheng Zhang, Stephen Lin, and Baining Guo. Swin transformer: Hierarchical vision transformer using shifted windows. In *Proceedings of the IEEE/CVF International Conference on Computer Vision (ICCV)*, 2021. 2, 4
- [35] Ilya Loshchilov and Frank Hutter. Decoupled weight decay regularization. In *International Conference on Learning Representations*, 2019. 6
- [36] Ziwei Luo, Fredrik K Gustafsson, Zheng Zhao, Jens Sjölund, and Thomas B Schön. Controlling vision-language models for universal image restoration. In *The Twelfth International Conference on Learning Representations*, 2023. 7, 8
- [37] D. Martin, C. Fowlkes, D. Tal, and J. Malik. A database of human segmented natural images and its application to evaluating segmentation algorithms and measuring ecological statistics. In *Proceedings Eighth IEEE International Conference on Computer Vision. ICCV 2001*, pages 416–423 vol.2, 2001. 5, 6
- [38] David Martin, Charless Fowlkes, Doron Tal, and Jitendra Malik. A database of human segmented natural images and its application to evaluating segmentation algorithms and measuring ecological statistics. In *ICCV*, 2001. 7, 8
- [39] David Martin, Charless Fowlkes, Doron Tal, and Jitendra Malik. A database of human segmented natural images and its application to evaluating segmentation algorithms and measuring ecological statistics. In *Proceedings Eighth IEEE International Conference on Computer Vision. ICCV 2001*, pages 416–423. IEEE, 2001. 7
- [40] Yusuke Matsui, Kota Ito, Yuji Aramaki, Azuma Fujimoto, Toru Ogawa, Toshihiko Yamasaki, and Kiyoharu Aizawa. Sketch-based manga retrieval using manga109 dataset. *Multimedia Tools Appl.*, 76(20):21811–21838, 2017. 5, 6
- [41] Seungjun Nah, Tae Hyun Kim, and Kyoung Mu Lee. Deep multi-scale convolutional neural network for dynamic scene deblurring. In *CVPR*, 2017. 8
- [42] Ben Niu, Weilei Wen, Wenqi Ren, Xiangde Zhang, Lianping Yang, Shuzhen Wang, Kaihao Zhang, Xiaochun Cao, and Haifeng Shen. Single image super-resolution via a holistic attention network. In *Computer Vision—ECCV 2020: 16th European Conference, Glasgow, UK, August 23–28, 2020, Proceedings, Part XII 16*, pages 191–207. Springer, 2020. 6
- [43] Vaishnav Potlapalli, Syed Waqas Zamir, Salman H Khan, and Fahad Shahbaz Khan. Promptir: Prompting for all-in-one image restoration. *NeurIPS*, 2023. 7, 8
- [44] Prajit Ramachandran, Niki Parmar, Ashish Vaswani, Irwan Bello, Anselm Levskaya, and Jon Shlens. Stand-alone self-attention in vision models. *Advances in neural information processing systems*, 32, 2019. 2
- [45] Renan A Rojas-Gomez, Teck-Yian Lim, Alex Schwing, Minh Do, and Raymond A Yeh. Learnable polyphase sampling for shift invariant and equivariant convolutional networks. *Advances in Neural Information Processing Systems*, 35:35755–35768, 2022. 4
- [46] Renan A Rojas-Gomez, Teck-Yian Lim, Minh N Do, and Raymond A Yeh. Making vision transformers truly shift-equivariant. In *Proceedings of the IEEE/CVF Conference on Computer Vision and Pattern Recognition*, pages 5568–5577, 2024. 2
- [47] Hyeonseok Son, Junyong Lee, Sunghyun Cho, and Seungyong Lee. Single image defocus deblurring using kernel-sharing parallel atrous convolutions. In *Proc. ICCV*, 2021. 6
- [48] Yuchuan Tian, Hanting Chen, Chao Xu, and Yunhe Wang. Image processing gnn: Breaking rigidity in super-resolution. In *Proceedings of the IEEE/CVF Conference on Computer Vision and Pattern Recognition*, pages 24108–24117, 2024. 2, 4, 5, 6
- [49] Hugo Touvron, Matthieu Cord, Matthijs Douze, Francisco Massa, Alexandre Sablayrolles, and Hervé Jégou. Training data-efficient image transformers & distillation through attention. In *International conference on machine learning*, pages 10347–10357. PMLR, 2021. 2

- [50] Jeya Maria Jose Valanarasu, Rajeev Yasarla, and Vishal M Patel. Transweather: Transformer-based restoration of images degraded by adverse weather conditions. In *Proceedings of the IEEE/CVF Conference on Computer Vision and Pattern Recognition*, pages 2353–2363, 2022. 8
- [51] Ashish Vaswani, Noam Shazeer, Niki Parmar, Jakob Uszkoreit, Llion Jones, Aidan N Gomez, Łukasz Kaiser, and Illia Polosukhin. Attention is all you need. *Advances in neural information processing systems*, 30, 2017. 2
- [52] Wenhai Wang, Enze Xie, Xiang Li, Deng-Ping Fan, Kaitao Song, Ding Liang, Tong Lu, Ping Luo, and Ling Shao. Pyramid vision transformer: A versatile backbone for dense prediction without convolutions. In *Proceedings of the IEEE/CVF international conference on computer vision*, pages 568–578, 2021. 2
- [53] Wenhai Wang, Enze Xie, Xiang Li, Deng-Ping Fan, Kaitao Song, Ding Liang, Tong Lu, Ping Luo, and Ling Shao. Pvt v2: Improved baselines with pyramid vision transformer. *Computational Visual Media*, 8(3):415–424, 2022. 2
- [54] Zhendong Wang, Xiaodong Cun, Jianmin Bao, Wengang Zhou, Jianzhuang Liu, and Houqiang Li. Uformer: A general u-shaped transformer for image restoration. In *Proceedings of the IEEE/CVF Conference on Computer Vision and Pattern Recognition (CVPR)*, pages 17683–17693, 2022. 6
- [55] Chen Wei, Wenjing Wang, Wenhan Yang, and Jiaying Liu. Deep retinex decomposition for low-light enhancement. In *British Machine Vision Conference*, 2018. 8
- [56] Haiping Wu, Bin Xiao, Noel Codella, Mengchen Liu, Xiyang Dai, Lu Yuan, and Lei Zhang. Cvt: Introducing convolutions to vision transformers. In *Proceedings of the IEEE/CVF international conference on computer vision*, pages 22–31, 2021. 2
- [57] Zhuofan Xia, Xuran Pan, Shiji Song, Li Erran Li, and Gao Huang. Vision transformer with deformable attention. In *Proceedings of the IEEE/CVF conference on computer vision and pattern recognition*, pages 4794–4803, 2022. 2
- [58] Renjun Xu, Kaifan Yang, Ke Liu, and Fengxiang He. $e(2)$ -equivariant vision transformer. In *Uncertainty in Artificial Intelligence*, pages 2356–2366. PMLR, 2023. 2
- [59] Yufei Xu, Qiming Zhang, Jing Zhang, and Dacheng Tao. Vita: Vision transformer advanced by exploring intrinsic inductive bias. *Advances in Neural Information Processing Systems*, 34, 2021. 2
- [60] Wenhan Yang, Robby T Tan, Jiashi Feng, Zongming Guo, Shuicheng Yan, and Jiaying Liu. Joint rain detection and removal from a single image with contextualized deep networks. *TPAMI*, 2019. 8
- [61] Xiaoyu Xiang Yawei Li, Yuchen Fan, Denis Demandolx, Rakesh Ranjan, Radu Timofte, and Luc Van Gool. Efficient and explicit modelling of image hierarchies for image restoration. In *Proceedings of the IEEE Conference on Computer Vision and Pattern Recognition*, 2023. 2, 5, 6, 7
- [62] Syed Waqas Zamir, Aditya Arora, Salman Khan, Munawar Hayat, Fahad Shahbaz Khan, Ming-Hsuan Yang, and Ling Shao. Multi-stage progressive image restoration. In *CVPR*, 2021. 1
- [63] Syed Waqas Zamir, Aditya Arora, Salman Khan, Munawar Hayat, Fahad Shahbaz Khan, and Ming-Hsuan Yang. Restormer: Efficient transformer for high-resolution image restoration. In *CVPR*, 2022. 2, 3, 6, 7, 8
- [64] Roman Zeyde, Michael Elad, and Matan Protter. On single image scale-up using sparse-representations. In *Curves and Surfaces: 7th International Conference, Avignon, France, June 24-30, 2010, Revised Selected Papers 7*, pages 711–730. Springer, 2012. 5, 6
- [65] Jinghao Zhang, Jie Huang, Mingde Yao, Zizheng Yang, Hu Yu, Man Zhou, and Feng Zhao. Ingredient-oriented multi-degradation learning for image restoration. In *Proceedings of the IEEE/CVF Conference on Computer Vision and Pattern Recognition*, pages 5825–5835, 2023. 7, 8
- [66] Jiale Zhang, Yulun Zhang, Jinjin Gu, Yongbing Zhang, Linghe Kong, and Xin Yuan. Accurate image restoration with attention retractable transformer. In *ICLR*, 2023. 7
- [67] Kai Zhang, Wangmeng Zuo, Yunjin Chen, Deyu Meng, and Lei Zhang. Beyond a Gaussian denoiser: Residual learning of deep CNN for image denoising. *IEEE Transactions on Image Processing*, 26(7):3142–3155, 2017. 7
- [68] Kai Zhang, Yawei Li, Wangmeng Zuo, Lei Zhang, Luc Van Gool, and Radu Timofte. Plug-and-play image restoration with deep denoiser prior. *IEEE Transactions on Pattern Analysis and Machine Intelligence*, 44(10):6360–6376, 2021. 1, 7
- [69] Lei Zhang, Xiaolin Wu, Antoni Buades, and Xin Li. Color demosaicking by local directional interpolation and nonlocal adaptive thresholding. *Journal of Electronic imaging*, 20(2): 023016–023016, 2011. 7
- [70] Qiming Zhang, Yufei Xu, Jing Zhang, and Dacheng Tao. Vitaev2: Vision transformer advanced by exploring inductive bias for image recognition and beyond. *arXiv preprint arXiv:2202.10108*, 2022. 2
- [71] Yulun Zhang, Kunpeng Li, Kai Li, Lichen Wang, Bineng Zhong, and Yun Fu. Image super-resolution using very deep residual channel attention networks. In *ECCV*, 2018. 1, 5, 6
- [72] Dian Zheng, Xiao-Ming Wu, Shuzhou Yang, Jian Zhang, Jian-Fang Hu, and Wei-shi Zheng. Selective hourglass mapping for universal image restoration based on diffusion model. In *Proceedings of the IEEE/CVF Conference on Computer Vision and Pattern Recognition*, 2024. 7, 8
- [73] Yupeng Zhou, Zhen Li, Chun-Le Guo, Song Bai, Ming-Ming Cheng, and Qibin Hou. Srformer: Permuted self-attention for single image super-resolution. In *Proceedings of the IEEE/CVF International Conference on Computer Vision*, pages 12780–12791, 2023. 2, 5, 6
- [74] Lei Zhu, Xinjiang Wang, Zhanhan Ke, Wayne Zhang, and Rynson WH Lau. Biformer: Vision transformer with bi-level routing attention. In *Proceedings of the IEEE/CVF conference on computer vision and pattern recognition*, pages 10323–10333, 2023. 2

Enhancing Image Restoration Transformer via Adaptive Translation Equivariance

Supplementary Material

A. Translation equivariance v.s. translation invariance

In this section, we briefly explore the difference between translation equivariance v.s. translation invariance.

Definition A.1. Translation Equivariance. We call function $\Phi(\cdot)$ is translation equivariant to translation operation $\mathcal{T}(\cdot)$, if $\Phi(\mathcal{T}(x)) = \mathcal{T}(\Phi(x))$, where x is the input signal.

Definition A.2. Translation Invariance. We call function $\Phi(\cdot)$ is translation invariant to translation operation $\mathcal{T}(\cdot)$, if $\Phi(\mathcal{T}(x)) = \Phi(x)$, where x is the input signal.

According to the aforementioned definitions, it can be inferred that a translation-equivariant operator ensures that when the input undergoes a translation, the output is translated accordingly. Equivariance maintains the spatial correspondence between the input and output. Conversely, a translation-invariant operator guarantees that the output remains unchanged when the input is translated, thereby ensuring stability against translation. Translation invariance highlights robustness to input variations.

In the context of image restoration tasks, where precise restoration is required at the pixel level, the model should maintain a degree of translation equivariance rather than translation invariance to enhance the fidelity of the restored image as we discussed in Sec. 1.

B. Proofs

In this section, we provide proofs of Theorem 3.2 and Theorem 3.3.

Proof of Theorem 3.2.

Proof. Given a function $\Phi(x)_i$ is transformed from $x_j = [i - b, i + b]$, where b is the sliding boundary, $\Phi(x)_i$ can be rewritten as follows.

$$\Phi(x)_i = \Phi(x_{j=[i-b, i+b]}), \quad (8)$$

where j is the index of the input signal x .

Given the translation operator $\mathcal{T}(\cdot)$, which satisfies $\mathcal{T}(x_j) = x_{j+\delta}$, where δ is a constant scalar.

$$\begin{aligned} \mathcal{T}(\Phi(x)_i) &= \Phi(x)_{i+\delta} \\ &= \Phi(x_{j=[i+\delta-b, i+\delta+b]}) \\ &= \Phi(\mathcal{T}(x)_{j=[i-b, i+b]}) \\ &= \Phi(\mathcal{T}(x))_i, \end{aligned} \quad (9)$$

which completes the proof.

Proof of Theorem 3.3.

Proof. Given functions $\Phi_1(\cdot)$ and $\Phi_2(\cdot)$ are translation equivariant to translation operation $\mathcal{T}(\cdot)$, according to Definition 3.1, we get:

$$\Phi_1(\mathcal{T}(x)) = \mathcal{T}(\Phi_1(x)), \quad (10)$$

$$\Phi_2(\mathcal{T}(x)) = \mathcal{T}(\Phi_2(x)). \quad (11)$$

Since the translation operation $\mathcal{T}(\cdot)$ is a linear operator, we can sum the above equations as follows.

$$\begin{aligned} \Phi_1(\mathcal{T}(x)) + \Phi_2(\mathcal{T}(x)) &= \mathcal{T}(\Phi_1(x)) + \mathcal{T}(\Phi_2(x)) \\ &= \mathcal{T}(\Phi_1(x) + \Phi_2(x)). \end{aligned} \quad (12)$$

It can be seen that the function $\Phi_1(\cdot) + \Phi_2(\cdot)$ is translation equivariant to translation operation $\mathcal{T}(\cdot)$.

When stacking the functions $\Phi_1(\cdot)$ and $\Phi_2(\cdot)$ in parallel,

$$\begin{aligned} \Phi_2(\Phi_1(\mathcal{T}(x))) &= \Phi_2(\mathcal{T}(\Phi_1(x))) \\ &= \mathcal{T}(\Phi_2(\Phi_1(x))). \end{aligned} \quad (13)$$

The function $\Phi_2(\Phi_1(\cdot))$ is also translation equivariant to translation operation $\mathcal{T}(\cdot)$, which completes the proof.